Singlet-triplet splitting, correlation, and entanglement of two electrons in quantum dot molecules

Lixin He, Gabriel Bester, and Alex Zunger

National Renewable Energy Laboratory, Golden, Colorado 80401, USA

Starting with an accurate pseudopotential description of the single-particle states, and following by configuration-interaction treatment of correlated electrons in vertically coupled, self-assembled InAs/GaAs quantum dot molecules, we show how simpler, popularly practiced approximations, depict the basic physical characteristics including the singlet-triplet splitting, degree of entanglement (DOE), and correlation. The mean-field-like single-configuration approaches such as Hartree-Fock and local spin density, lacking correlation, incorrectly identify the ground-state symmetry and give inaccurate values for the singlet-triplet splitting and the DOE. The Hubbard model gives qualitatively correct results for the ground-state symmetry and singlet-triplet splitting, but produces significant errors in the DOE because it ignores the fact that the strain is asymmetric even if the dots within a molecule are identical. Finally, the Heisenberg model gives qualitatively correct ground-state symmetry and singlet-triplet splitting only for rather large interdot separations, but it greatly overestimates the DOE as a consequence of ignoring the electron double occupancy effect.

I. INTRODUCTION

Two vertically[1,2] or laterally[3] coupled quantum dots containing electrons, holes, or an exciton constitute the simplest solid structure proposed for the basic gate operations of quantum computing.[4,5] The operating principle is as follows: when two dots couple to each other, bonding and antibonding "molecular orbitals" (MOs) ensue from the single-dot orbitals $\{\chi_i\}$ of the top (T) and bottom (B) dots: $\psi(\sigma_g) = \chi_T(s) + \chi_B(s)$ is the σ-type bonding and $\psi(\sigma_u) = \chi_T(s) - \chi_B(s)$ is the σ-type antibonding state. Similarly, $\psi(\pi_u) = \chi_T(p) + \chi_B(p)$ and $\psi(\pi_g) = \chi_T(p) - \chi_B(p)$ are the "π" bonding and antibonding states constructed from the "p" single-dot orbitals of top and bottom dots, respectively. Injection of two electrons into such a diatomic "dot molecule" creates different spin configurations such as $|\sigma_g^\uparrow, \sigma_u^\uparrow\rangle$ or $|\sigma_g^\downarrow, \sigma_u^\downarrow\rangle$, depicted in Fig. 1(a). In the absence of spin-orbit coupling, these two-electron states are either spin-singlet or spin-triplet states with energy separation J_{S-T}. Loss and DiVincenzo[5] proposed a "swap gate" base on a simplified model, where two localized spins have Heisenberg coupling, $H = J_{S-T}(t)\vec{S}_1 \cdot \vec{S}_2$. Here $\vec{S}_1$ and $\vec{S}_2$ are the spin-1/2 operators for the two localized electrons. The effective Heisenberg exchange splitting $J_{S-T}(t)$ is a function of time t, which is measured as the difference in the energy between the spin-triplet state with the total spin $S=1$ and the spin-singlet state with $S=0$. The "state swap time" is $\tau \sim 1/J_{S-T}$. An accurate treatment of the singlet-triplet splitting J_{S-T} and the degree of entanglement carried by the two electrons is thus of outmost importance for this proposed approach to quantum computations.

Theoretical models, however, differ in their assessment of the magnitude and even the sign of the singlet-triplet energy difference J_{S-T} that can be realized in a quantum dot molecule (QDM) with two electrons. Most theories have attempted to model dot molecules made of large (50–100 nm), electrostatically confined[6–8] dots having typical single-particle electronic levels separation of 1–5 meV, with larger (or comparable) interelectronic Coulomb energies

$J_{ee} \sim 5$ meV. The central approximation used almost universally is that the single-particle physics is treated via particle-in-a-box effective-mass approximation (EMA), where multiband and intervally couplings are neglected. (In this work, we will deviate from this tradition, see below.) Many-body treatments of this simplified EMA model range from phenomenological Hubbard[9] or Heisenberg[5,9] models using empirical input parameters, to microscopic Hartree-Fock (HF),[10–12] local spin densities (LSD) approximation,[13,14] and configuration interaction (CI) method.[2,15]

The LSD-EMA (Refs. 13 and 14) can treat easily up to a few tens of electrons in the quantum dot molecules, but has shortcomings for treating strongly correlated electrons, predicting for a dot molecule loaded with two electrons that the triplet state is *below* the singlet in the weak coupling region,[13] as well as incorrectly mixing singlet (spin unpolarized) and triplet (spin polarized) even in the absence of spin-orbit coupling. Since in mean-field approaches like LSD or HF, the two electrons are forced to occupy the same molecular orbital delocalized on both dots, the two-electron states are purely unentangled.

The restricted (R) HF method (RHF-EMA) shares similar failures with LSD, giving a triplet as the ground state at large
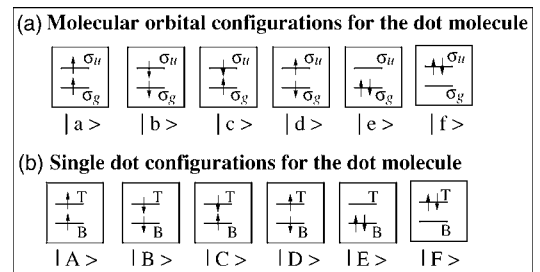

FIG. 1. Possible configurations for two electrons in two vertically coupled quantum dots. (a) Spin configurations in the MO basis. σ_g and σ_u indicate the bonding and antibonding states, respectively. (b) Spin configurations in the dot-localized basis. "T" and "B" indicate the top and bottom dots.

interdot separation. The unrestricted (U) HF (Ref. 11) corrects some of the problems of RHF by relaxing the requirement of (i) two electrons of different spins occupying the same spatial orbital, and (ii) the single-particle wave functions have the symmetry of the external confining potential. The UHF-EMA correctly give the singlet lower in energy than the triplet,[12] and can also predict Mott localization of the electrons in the dot molecule, which breaks the many-particle symmetry.[11] However, since in UHF, the symmetry-broken wave functions are only the eigenstates of the z component of total spin $S = s_1 + s_2$, but not of S^2, the UHF-EMA incorrectly mixes the singlet and triplet.[11,12] For the simple case of dot molecules having inversion symmetry, (e.g., molecules made of spherical dots but not of vertical lens-shaped dots), assuming EMA and neglecting spin-orbit coupling, there is an *exact* symmetry. For this case, Refs. 16 and 17 indeed were able to project out the eigenstates of S^2, yielding good spin quantum numbers and lower energy. However, for vertically coupled lens shaped quantum dots (i.e., realistic self-assembled systems) or even for spherical dots, but in the presence of spin-orbit coupling, there is no exact symmetry. In this case, configurations with different symmetries may couple to each other. To get the correct energy spectrum and many-body wave functions, a further variation has to be done after the projection, e.g., using the generalized valence bond (GVB) method.[18] For this case and other cases a CI approach is needed.

The CI-EMA has been proven[2,15] to be accurate for treating few-electron states in large electrostatic dot molecules, and predicts the correct ground state. Finally, recent quantum Monte Carlo EMA calculations[19] also show that the singlet is below the triplet.

The above discussion pertained to large (50–100 nm) electrostatic-confined dots. Recently, dot molecules have been fabricated[20,21] from self-assembled InAs/GaAs, offering a much larger J_{S-T}. Such dots have much smaller confining dimensions (height of only 2–5 nm), showing a typical spacing between electron levels of 40–60 meV, *smaller* interelectronic Coulomb energies $J_{ee} \sim 20$ meV, and exchange energies of $K_{ee} \sim 3$ meV. Such single dots have been accurately modeled[22] via atomistic pseudopotential theories, applied to the single-particle problem (including multiband and intervalley couplings as well as nonparabolicity, thus completely avoiding the effective-mass approximation). The many-particle problem is then described via the all-bound-state configuration-interaction method. Here we use this methodology to study the singlet-triplet splitting in vertically stacked self-assembled InAs/GaAs dots. We calculate first the singlet-triplet splitting vs interdot separation, finding the singlet to be below the triplet. We then simplify our model in successive steps, reducing the sophistication with which interelectronic correlation is described and showing how these previously practiced approximations[10–14] lead to different values of J_{S-T}, including its sign reversal. This methodology provides insight into the electronic processes which control the singlet-triplet splitting in dot molecules.

The remainder of the paper is arranged as follows. In Sec. II we provide technical details regarding the methodology we use for the calculations. We then compare the singlet-triplet splitting, degree of entanglement, and correlation of
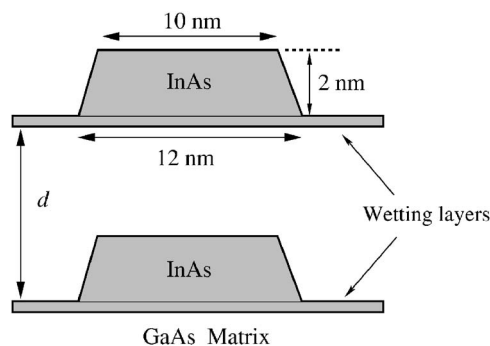

FIG. 2. Geometry of the two vertically coupled quantum dot molecule. The interdot distance d is measured from wetting layer to wetting layer.

two-electron states in different levels of approximations in Sec. III. Finally, we summarize in Sec. IV.

II. METHODS

A. Geometry and strain relaxation

We consider a realistic dot-molecule geometry[4] shown in Fig. 2, which has recently been used in studying exciton entanglement[4,23] and two-electron states.[24] Each InAs dot is 12 nm wide and 2 nm tall, with one monolayer InAs "wetting layer," and compressively strained by a GaAs matrix. Even though experimentally grown dot molecules often have slightly different size and composition profile for each dot within the molecule, here we prefer to consider identical dots, so as to investigate the extent of symmetry breaking due to many-body effects in the extreme case of identical dots. The minimum-strain configuration is achieved at each interdot separation d, by relaxing the positions $\{\mathbf{R}_{n,\alpha}\}$ of all (dot+matrix) atoms of type α at site n, so as to minimize the bond-bending and bond-stretching energy using the valence force field (VFF) method.[25,26] This shows that both dots have large and nearly constant hydrostatic strain inside the dots which decays rapidly outside.[24] However, even though the dots comprising the molecule are geometrically identical, the strain on the two dots is different since the molecule lacks inversion symmetry. In fact, we found that the top dot is slightly more strained than the bottom dot. Not surprisingly, the GaAs region *between* the two dots is more severely strained than in other parts of the matrix, as shown in Fig. 1 of Ref. 24 and as the two dots move apart, the strain between them decreases.

B. Calculating the single-particle states

The single-particle electronic energy levels and wave functions are obtained by solving the Schrödinger equations in a pseudopotential scheme,

$$\left[-\frac{1}{2}\nabla^2 + V_{\text{ps}}(\mathbf{r}) \right] \psi_i(\mathbf{r}) = \epsilon_i \psi_i(\mathbf{r}), \tag{1}$$

where the total electron-ion potential $V_{\text{ps}}(\mathbf{r})$ is a superposition of local, screened atomic pseudopotentials $v_a(\mathbf{r})$, i.e.,

$V_{ps}(\mathbf{r}) = \Sigma_{n,\alpha} v_\alpha(\mathbf{r} - \mathbf{R}_{n,\alpha})$. The pseudopotentials used for InAs/GaAs are identical to those used in Ref. 27 and were tested for different systems.[23,27,28] We ignored spin-orbit coupling in the InAs/GaAs quantum dots, since it is extremely small for electrons treated here (but not for holes which we do not discuss in the present work). Without spin-orbit coupling, the states of two electrons are either pure singlet or pure triplet. However, if a spin-orbit coupling is introduced, the singlet state would mix with triplet state.

Equation (1) is solved using the "linear combination of Bloch bands" (LCBB) method,[29] where the wave functions ψ_i are expanded as

$$\psi_i(\mathbf{r}) = \sum_{n,\mathbf{k}} \sum_\lambda C_{n,\mathbf{k}}^{(\lambda)} \phi_{n,\mathbf{k},\overleftrightarrow{\epsilon}}^{(\lambda)}(\mathbf{r}). \qquad (2)$$

In the above equation, $\{\phi_{n,k,\overleftrightarrow{\epsilon}}^{(\lambda)}(\mathbf{r})\}$ are the bulk Bloch orbitals of band index n and wave vector $\mathbf{k}$ of material λ (=InAs, GaAs), strained uniformly to strain $\overleftrightarrow{\epsilon}$. The dependence of the basis functions on strain makes them variationally efficient. (Note that the potential $V_{ps}(\mathbf{r})$ itself also has the inhomogeneous strain dependence through the atomic position $\mathbf{R}_{n,\alpha}$.) We use for the basis set $\overleftrightarrow{\epsilon}=0$ for the (unstrained) GaAs matrix material, and an average $\overleftrightarrow{\epsilon}$ value from VFF for the strained dot material (InAs). For the InAs/GaAs system, we use $n=2$ (including spin) for electron states on a $6 \times 6 \times 28$ k mesh. A single dot with the geometry of Fig. 2 (base=12 nm and height=2 nm) has three bound electron states (s, p_1, and p_2) and more than ten bound hole states. The lowest exciton transition in the single dot occurs at energy 1.09 eV. For the dot molecule the resulting single-particle states are, in order of increasing energy, σ_g and σ_u (bonding and antibonding combination of the s-like single-dot orbitals), and the doubly (nearly) degenerate π_u and π_g, originating from doubly (nearly) degenerate "p" orbitals (split by a few meV) in a single dot. Here, we use the symbols g and u to denote symmetric and antisymmetric states, even though in our case the single-particle wave functions are actually asymmetric.[24] We define the difference between the respective dot molecule eigenvalues as $\Delta_\sigma = \epsilon(\sigma_u) - \epsilon(\sigma_g)$ and $\Delta_\pi = \epsilon(\pi_g) - \epsilon(\pi_u)$.

C. Calculating the many-particle states

The Hamiltonian of interacting electrons can be written as

$$H = \sum_{i\sigma} \epsilon_i \psi_{i\sigma}^\dagger \psi_{i\sigma} + \frac{1}{2} \sum_{ijkl} \sum_{\sigma,\sigma'} \Gamma_{kl}^{ij} \psi_{i\sigma}^\dagger \psi_{j\sigma'}^\dagger \psi_{k\sigma'} \psi_{l\sigma}, \qquad (3)$$

where $\psi_i = \sigma_u, \sigma_g, \pi_u, \pi_g$ are the single-particle energy levels of the ith molecular orbital, while $\sigma, \sigma' = 1, 2$ are spin indices. The Γ_{kl}^{ij} are the Coulomb integrals between molecular orbitals ψ_i, ψ_j, ψ_k, and ψ_l,

$$\Gamma_{kl}^{ij} = \int \int d\mathbf{r}\, d\mathbf{r}' \frac{\psi_i^*(\mathbf{r}) \psi_j^*(\mathbf{r}') \psi_k(\mathbf{r}') \psi_l(\mathbf{r})}{\epsilon(\mathbf{r} - \mathbf{r}') |\mathbf{r} - \mathbf{r}'|}. \qquad (4)$$

The $J_{ij} = \Gamma_{ji}^{ij}$ and $K_{ij} = \Gamma_{ij}^{ij}$ are diagonal Coulomb and exchange integrals, respectively. The remaining terms are called off-diagonal or scattering terms. All Coulomb integrals are calculated numerically from atomistic wave functions.[30] We use a phenomenological, position-dependent dielectric function $\epsilon(\mathbf{r} - \mathbf{r}')$ to screen the electron-electron interaction.[30]

We solve the many-body problem of Eq. (3) via the CI method, by expanding the N-electron wave function in a set of Slater determinants, $|\Phi_{e_1,e_2,...,e_N}\rangle = \phi_{e_1}^\dagger \phi_{e_2}^\dagger \cdots \phi_{e_N}^\dagger |\Phi_0\rangle$, where $\phi_{e_i}^\dagger$ creates an electron in the state e_i. The νth many-particle wave function is then the linear combinations of the determinants,

$$|\Psi_\nu\rangle = \sum_{e_1,e_2,...,e_N} A_\nu(e_1, e_2, ..., e_N) |\Phi_{e_1,e_2,...,e_N}\rangle. \qquad (5)$$

In this paper, we only discuss the two-electron problem, i.e., $N=2$. Our calculations include all possible Slater determinants for the six single-particle levels.

D. Calculating pair-correlation functions and degree of entanglement

We calculate in addition to the energy spectrum and the singlet-triplet splitting J_{S-T} also the pair-correlation functions and the degrees of entanglement (DOE). The pair-correlation function $P_\nu(\mathbf{r}, \mathbf{r}')$ for an N-particle system is defined as the probability of finding an electron at $\mathbf{r}'$, given that the other electron is at $\mathbf{r}$, i.e.,

$$P_\nu(\mathbf{r}, \mathbf{r}') = \int d\mathbf{r}_3 \cdots d\mathbf{r}_N |\Psi_\nu(\mathbf{r}, \mathbf{r}', \mathbf{r}_3, ..., \mathbf{r}_N)|^2, \qquad (6)$$

where, $\Psi_\nu(\mathbf{r}_1, ..., \mathbf{r}_N)$ is the N-particle wave function of state ν. For two electrons, the pair-correlation function is just $P_\nu(\mathbf{r}, \mathbf{r}') = |\Psi_\nu(\mathbf{r}, \mathbf{r}')|^2$.

The degree of entanglement (DOE) is one of the most important quantities for successful quantum gate operations. For *distinguishable* particles such as electron and hole, the DOE can be calculated from von Neumann–entropy formulation.[31–34] However, for *indistinguishable* particles, there are some subtleties[35–41] for defining the DOE since it is impossible to separate the two *identical* particles. Recently, a quantum correlation function[35] has been proposed for indistinguishable particles using the Slater decompositions.[42] We adapt this quantum correlation function to define the DOE for indistinguishable fermions as

$$S = -\sum_u z_i^2 \log_2 z_i^2, \qquad (7)$$

where z_i are Slater decomposition coefficients. The details of deriving Eq. (7) are given in Appendix A. We also show in Appendix A that the DOE measure of Eq. (7) reduces to the usual von Neumann–entropy formulation when the two electrons are far from each other.

III. RESULTS

Figure 3 shows the bonding-antibonding splitting $\Delta_\sigma(d)$ between the molecular orbitals vs interdot separation d measured from one wetting layer to the other, showing also the value $\delta_{sp} = \epsilon_p - \epsilon_s$ of the splitting between the p and s orbital energies of a *single dot* (i.e., $d \rightarrow \infty$). The bonding-
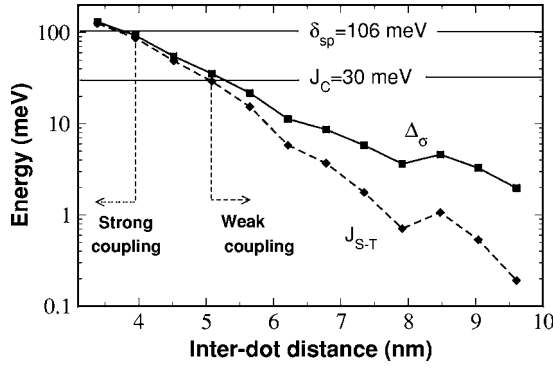
FIG. 3. The bonding-antibonding splitting $\Delta_\sigma = \epsilon(\sigma_g) - \epsilon(\sigma_u)$ (solid line) and singlet-triplet splitting $J_{S-T} = E(^3\Sigma) - E(^1\Sigma_g^{(a)})$ (dashed line) vs interdot distance d. We also show the single-dot s, p orbitals splitting $\delta_{sp} = e_s - e_p$ and the s orbital Coulomb interaction J_C. We define "strong coupling" by $\Delta_\sigma \sim \delta_{sp}$ (<4 nm) and "weak coupling," $\Delta_\sigma \ll \delta_{sp}$ (>5 nm).

antibonding splitting decays approximately exponentially as $\Delta_\sigma = 2.87 \exp(-d/1.15)$ eV between $d \sim 4$ and 8 nm. The result of bonding-antibonding splitting includes two competing effects. On one hand, large interdot distance d reduces the coupling between the two dots; on the other hand, the strain between the dots is also reduced, leading to a lower tunneling barrier, thus increasing coupling. The local maximum of Δ_σ at $d = 8.5$ nm is a consequence of the this competition. Recent experiments[20,21] show the bonding-antibonding splitting of about 4 meV at $d = 11.5$ nm for vertically coupled InAs/GaAs quantum dot molecules, of similar magnitude as the value obtained here (~ 1 meV), considering that the measured dot molecule is larger (height/base=4 nm/40 nm rather than 2 nm/12nm in our calculations) and possibly asymmetric. We also give in Fig. 3 the interelectronic Coulomb energy J_C of a *single-dot s* orbital. We define the *strong-coupling* region as $\Delta_\sigma \approx \delta_{sp}$, and the *weak-coupling* region $\Delta_\sigma \ll \delta_{sp}$. We see in Fig. 3 strong coupling for $d \lesssim 4$ nm, and weak coupling for $d \gtrsim 5$ nm. In the weak-coupling region, the π levels are well above the σ levels. We also define "strong confinement" as $\delta_{sp} > J_C$, and weak confinement as the reverse inequality. Figure 3 shows that our dot is
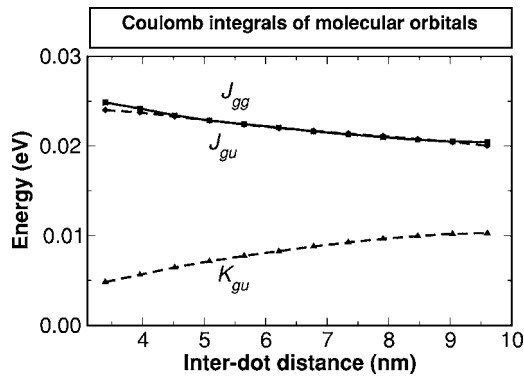

FIG. 4. Selected Coulomb integrals for molecular orbitals. J_{gg} is the self-Coulomb energy of the σ_g orbital and J_{gu} is the Coulomb energy between σ_g and σ_u orbitals, while K_{gu} is the exchange energy between σ_g and σ_u orbitals.
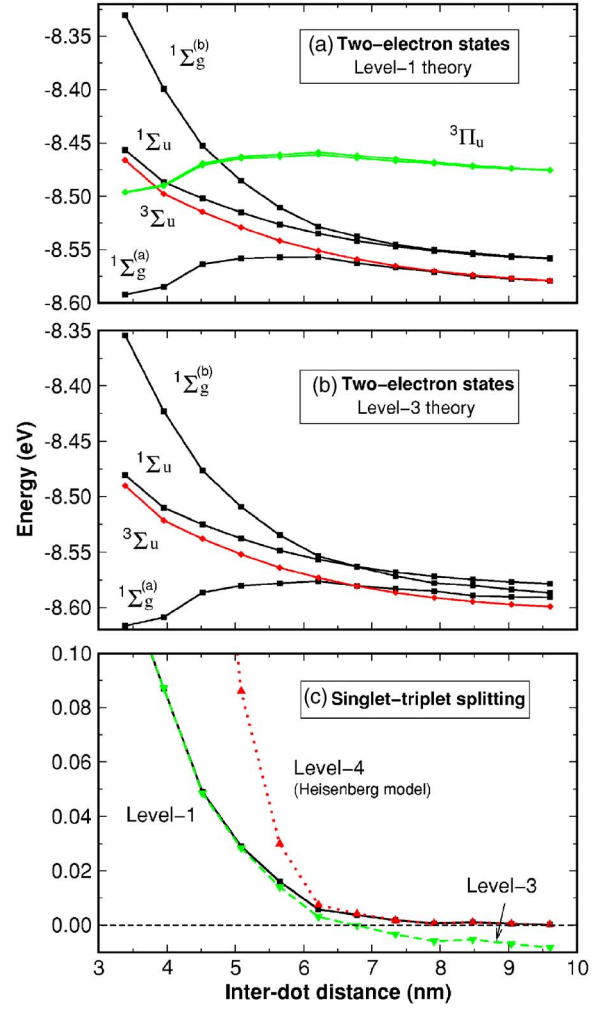

FIG. 5. (Color online) (a) Two-electron states calculated from CI using all confined MO from LCBB (level 1), including the singlet $^1\Sigma_g^{(a)}$, $^1\Sigma_u$, $^1\Sigma_g^{(b)}$ states and the threefold degenerated triplet states $^3\Sigma_u$ as well as two threefold degenerated triplet states $^3\Pi_u$. (b) Two electron states calculated from the single-configuration approximation (level 3). (c) Comparison of the singlet-triplet splitting calculated from level-1, -3, and -4 theories.

in the strong-confinement regime. In contrast, electrostatic dots[6–8] are in the weak confinement regime.

We next discuss the two-electron states in the QDMs and examine several different approximations which we call levels 1–4, by comparing the properties of the ground states, the singlet-triplet energy separation J_{S-T} and the pair-correlation functions as well as the degree of entanglement for each state. Starting from our most complete model (level 1) and simplifying it in successive steps, we reduce the sophistication with which interelectronic correlation is described and show how these previously practiced approximations lead to different values of J_{S-T} (including its sign reversal), and different degree of entanglement. This methodology provides insight into the electronic features which control singlet-triplet splitting and electron-electron entanglement in dot molecules.
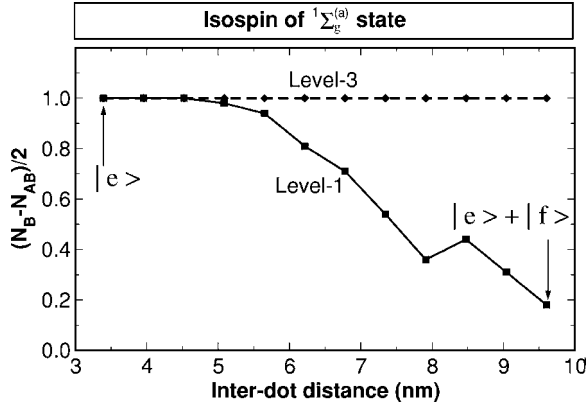
FIG. 6. Isospin, defined as the difference in the number of electrons occupying the bonding (N_B) and antibonding (N_{AB}) states, of the $^1\Sigma_g^{(a)}$ state in level-1 and level-3 theories.

A. Level-1 theory: All-bound-state configuration interaction

We first study the two-electron states by solving the CI Eq. (5), using all confined molecular orbitals σ_g, σ_u and π_g, π_u, to construct the Slater determinants. This gives a total of 66 Slater determinants. The continuum states are far above the bound state, and are thus not included in the CI basis. Figure 4 shows some important matrix elements, including J_{gg} (Coulomb energy of σ_g MO), J_{gu} (Coulomb energy between σ_g and σ_u), and K_{gu} (exchange energy between σ_g and σ_u). The Coulomb energy between σ_u MO, J_{uu} is nearly identical to J_{gg} and therefore is not plotted. Diagonalizing the all-bound-state CI problem gives the two-particle states, shown in Fig. 5(a). We show all six Σ states (where both electrons occupy the σ states) and the two lowest threefold degenerate $^3\Pi_u$ states (where one electron occupies the σ_g and one occupies one of the π levels). We observe that:

(i) The ground state is singlet $^1\Sigma_g^{(a)}$ for all dot-dot distances. However, the character of the state is very different at different interdot separation d, which can be analyzed by the isospin of the state,[43] defined as the difference in the number of electrons occupying the bonding (N_B) and antibonding N_{AB}) states in a given CI state, i.e., $I_z = (N_B - N_{AB})/2$, where N_B and N_{AB} are obtained from Eq. (5). As shown in Fig. 6, $I_z(d)$ of the $^1\Sigma_g^{(a)}$ state is very different at different interdot distances: At small interdot distance, the dominant configuration of the ground state is $|\sigma_g^\uparrow, \sigma_g^\downarrow\rangle$ (both electrons occupy bonding state and $N_B = 2$), and $I_z \sim 1$. However, in the weak-

coupling region, there is significant mixing of bonding σ_g and antibonding states σ_u, and I_z is smaller than 1, e.g., $I_z \sim 0.2$ at $d = 9.5$ nm. At infinite separation, where the bonding and antibonding states are degenerate, one expects $I_z \rightarrow 0$.

(ii) Next to the ground state, we find in Fig. 5(a) the threefold degenerate triplet states $^3\Sigma_u$, with $S_z = 1, -1$, and 0. In the absence of spin-orbit coupling, triplet states will not couple to singlet states. If we include spin-orbit coupling, the triplet may mix with the singlet state, and the degeneracy will be lifted. At large interdot distances, the ground-state singlet $^1\Sigma_g^{(a)}$ and triplet states $^3\Sigma_u$ are degenerate. The splitting of total CI energy between ground-state singlet and triplet $J_{S-T} = E(^3\Sigma) - E(^1\Sigma_g)$ is plotted in Fig. 3 on a logarithmic scale. As we can see, J_{S-T} also decays approximately exponentially between 4 and 8 nm, and can be fitted as $J_{S-T} = 5.28 \exp(-d/0.965)$eV. The decay length of 0.965 nm is shorter than the decay length 1.15 nm of Δ_σ. At small interdot separations, $J_{S-T} \sim \Delta_\sigma$ in Fig. 3, as expected from a simple Heitler-London model.[9]

(iii) The two excited singlet states originating from the occupation of σ_u antibonding states, $^1\Sigma_u$ and $^1\Sigma_g^{(b)}$ are further above the $^3\Sigma_u$ state.

(iv) The lowest $^3\Pi_u$ states are all triplet states. They are energetically very close to each other since we have two nearly degenerate π_u MO states. In the weak-coupling region, the Π_u states are well above the Σ states, as a consequence of large single-particle energy difference $\epsilon(\pi_u) - \epsilon(\sigma_u)$. However, the Π_u, and $^1\Sigma_g^{(b)}$ cross at about 4.5 nm, where the single-particle MO level π_u is still much higher than σ_u. In this case, the Coulomb correlations have to be taken into account.

In the following sections, we enquire as to possible, popularly practiced simplifications over the all-bound-states CI treatment.

B. Level-2 theory: Reduced CI in the molecular basis

In level-2 theory, we will reduce the full 66×66 CI problem of level 1 to one that includes only the σ_g and σ_u basis, giving a 6×6 CI problem. The six many-body basis states are shown in Fig. 1(a), $|a\rangle = |\sigma_g^\uparrow, \sigma_u^\uparrow\rangle$, $|b\rangle = |\sigma_g^\downarrow, \sigma_u^\downarrow\rangle$, $|c\rangle = |\sigma_g^\uparrow, \sigma_u^\downarrow\rangle$, $|d\rangle = |\sigma_g^\downarrow, \sigma_u^\uparrow\rangle$, $|e\rangle = |\sigma_g^\uparrow, \sigma_g^\downarrow\rangle$, $|f\rangle = |\sigma_u^\uparrow, \sigma_u^\downarrow\rangle$. In this basis set, the CI problem is reduced to a 6×6 matrix eigenvalue equation,

$$H = \begin{pmatrix} \epsilon_g + \epsilon_u + J_{gu} - K_{gu} & 0 & 0 & 0 & 0 & 0 \\ 0 & \epsilon_g + \epsilon_u + J_{gu} - K_{gu} & 0 & 0 & 0 & 0 \\ 0 & 0 & \epsilon_g + \epsilon_u + J_{gu} & -K_{gu} & -\Gamma_{gg}^{gu} & -\Gamma_{uu}^{gu} \\ 0 & 0 & -K_{gu} & \epsilon_g + \epsilon_u + J_{gu} & \Gamma_{gg}^{gu} & \Gamma_{uu}^{gu} \\ 0 & 0 & -\Gamma_{gu}^{gg} & \Gamma_{gu}^{gg} & 2\epsilon_g + J_{gg} & \Gamma_{uu}^{gg} \\ 0 & 0 & -\Gamma_{gu}^{uu} & \Gamma_{gu}^{uu} & \Gamma_{gg}^{uu} & 2\epsilon_u + J_{uu} \end{pmatrix}, \quad (8)$$

where ϵ_g and ϵ_u are the single-particle energy levels for the MOs $|\sigma_g\rangle$ and $|\sigma_u\rangle$, respectively. In the absence of spin-orbit coupling, the triplet states $|a\rangle$ and $|b\rangle$ are not coupled to *any* other states, as required by the total spin conservation, and thus they are already eigenstates. The rest of the matrix can be solved using the integrals calculated from Eq. (4). The results of the 6×6 problem were compared (not shown) to the all-bound-state CI results: We find that the Σ states of level-2 theory are very close to those of the all-bound-state CI calculations, indicating a small coupling between σ and π orbitals in the *strong confinement* region. We thus do not show graphically the results of level 2. However, since we use only σ orbitals, the Π states of level 1 [Fig. 5(a)] are absent in level-2 theory. Especially, the important feature of crossover between Σ and Π_u states at 4 and 4.5 nm is missing.

C. Level-3 theory: Single-configuration in the molecular basis

As is well known, mean-field-like treatments such as RHF and LSD usually give incorrect dissociation behavior of molecules, as the correlation effects are not adequately treated. Given that RHF and LSD are widely used in studying QMDs,[10,13,14] it is important to understand under which circumstance the methods will succeed and under which circumstance they will fail in describing the few-electron states in a QDM. In level-3 theory, we thus mimic the mean-field theory by further ignoring the *off-diagonal* Coulomb integrals in Eq. (8) of level-2 theory, i.e., we assume $\Gamma_{uu}^{gu} = \Gamma_{gg}^{gu} = \Gamma_{gg}^{uu} = 0$. This approximation is equivalent to ignoring the coupling between different configurations, and is thus called "single-configuration" (SC) approximation. At the SC level, we have very simple analytical solutions of the two-electron states,

$$E\left({}^1\Sigma_g^{(a)}\right) = 2\epsilon_g + J_{gg}; \quad \left|{}^1\Sigma_g^{(a)}\right\rangle = |e\rangle, \quad (9)$$

$$E\left({}^3\Sigma_u\right) = (\epsilon_g + \epsilon_u) + J_{gu} - K_{gu}; \quad \begin{cases} \left|{}^3_+\Sigma_u\right\rangle = |a\rangle, \\ \left|{}^3_-\Sigma_u\right\rangle = |b\rangle, \\ \left|{}^3_0\Sigma_u\right\rangle = |c\rangle - |d\rangle, \end{cases} \quad (10)$$

$$E\left({}^1\Sigma_u\right) = (\epsilon_g + \epsilon_u) + J_{gu} + K_{gu}; \quad \left|{}^1\Sigma_u\right\rangle = |c\rangle + |d\rangle, \quad (11)$$

$$E\left({}^1\Sigma_g^{(b)}\right) = 2\epsilon_u + J_{uu}; \quad \left|{}^1\Sigma_g^{(b)}\right\rangle = |f\rangle. \quad (12)$$

The energies are plotted in Fig. 5(b). When comparing the Σ states of the SC approach to the all-bound-state CI results in Fig. 5(a), we find good agreement in the strong-coupling region for $d \leq 5$ nm (see Fig. 3). However, the SC approximation fails qualitatively at larger inter-dot separations in two aspects: (i) The order of singlet state ${}^1\Sigma_g^{(a)}$ and triplet state ${}^3\Sigma_u$ is reversed [see Figs. 5(b) and 5(c)]. (ii) The ${}^1\Sigma_g^{(a)}$ and ${}^3\Sigma_u$ states fail to be degenerate at large interdot separation. This lack of degeneracy is also observed for ${}^1\Sigma_g^{(b)}$ and ${}^1\Sigma_u$. These failures are due to the absence of correlations in the SC approximation. Indeed as shown in Fig. 6, the accurate level-1 ground-state singlet has considerable mixing of

antibonding states, i.e., $I_z \to 0$ at large d. However, in the SC approximation both electrons are *forced* to occupy the σ_g orbital in the lowest singlet state ${}^1\Sigma_g^{(a)}$ as a consequence of the lack of the coupling between the configuration $|e\rangle$ of Fig. 1(a) and other configurations. As a result, in level-3 theory, the isospins are forced to be $I_z = 1$ for ${}^1\Sigma_g^{(a)}$ at all interdot distances d, which pushes the singlet energy higher than the triplet.

D. Level-4 theory: Hubbard model and Heisenberg model in a dot-centered basis

The Hubbard model and the Heisenberg model are often used[5] to analyze entanglement and gate operations for two spins qubits in a QDM. Here, we analyze the extent to which such approaches can correctly capture the qualitative physics given by more sophisticated models. Furthermore, by doing so, we obtain the parameters of the models from realistic calculations.

1. Transforming the states to a dot-centered basis

Unlike the level-1–3 theories, the Hubbard and the Heisenberg models are written in a dot-centered basis as shown in Fig. 1(b), rather than in the molecular basis of Fig. 1(a). In a dot-centered basis, the Hamiltonian of Eq. (3) can be rewritten as

$$H = \sum_{\eta_1, \eta_2} \sum_{\sigma} (e_{\eta_1} \delta_{\eta_1 \eta_2} + t_{\eta_1 \eta_2}) \chi_{\eta_1, \sigma}^\dagger \chi_{\eta_2 \sigma}$$
$$+ \frac{1}{2} \sum_{\eta_1, \ldots, \eta_4} \sum_{\sigma, \sigma'} \widetilde{\Gamma}_{\eta_3, \eta_4}^{\eta_1, \eta_2} \chi_{\eta_1, \sigma}^\dagger \chi_{\eta_2, \sigma'}^\dagger \chi_{\eta_3, \sigma'} \chi_{\eta_4, \sigma}, \quad (13)$$

where $\eta = (l, p)$ and $\chi_{\eta, \sigma}^\dagger$ creates an electron in the $l = (s, p, \ldots)$ orbital on the $p = (T, B)$ dot with spin σ that has single-particle energy e_η. Here, $t_{\eta_1 \eta_2}$ is the coupling between the η_1 and η_2 orbitals, and $\widetilde{\Gamma}_{\eta_3, \eta_4}^{\eta_1, \eta_2}$ is the Coulomb integral of single-dot orbitals χ_{η_1}, χ_{η_2}, χ_{η_3}, and χ_{η_4}.

We wish to construct a Hubbard Hamiltonian whose parameters are taken from the fully atomistic single-particle theory. To obtain such parameters in Eq. (13) including e_η, $t_{\eta_1 \eta_2}$, and $\widetilde{\Gamma}_{\eta_3, \eta_4}^{\eta_1, \eta_2}$, we resort to a Wannier-like transformation, which transform the "molecular" orbitals [Fig. 1(a)] into single-dot "atomic" orbitals [Fig. 1(b)]. The latter dot-centered orbitals are obtained from a unitary rotation of the *molecular* orbitals ψ_i, i.e.,

$$\chi_\eta = \sum_{i=1} \mathcal{U}_{\eta, i} \psi_i, \quad (14)$$

where ψ_i is the ith molecular orbitals, χ_η is the single dot-centered orbitals, and $\mathcal{U}$ are unitary matrices, i.e., $\mathcal{U}^\dagger \mathcal{U} = I$. We chose the unitary matrices that maximize the total orbital self-Coulomb energy. The procedure of finding these unitary matrices is described in detail in Appendix B. The dot-centered orbitals constructed this way are approximately invariant to the change of coupling between the dots.[44] Once we have the $\mathcal{U}$ matrices, we can obtain all the parameters in Eq. (13) by transforming them from the molecular basis. The
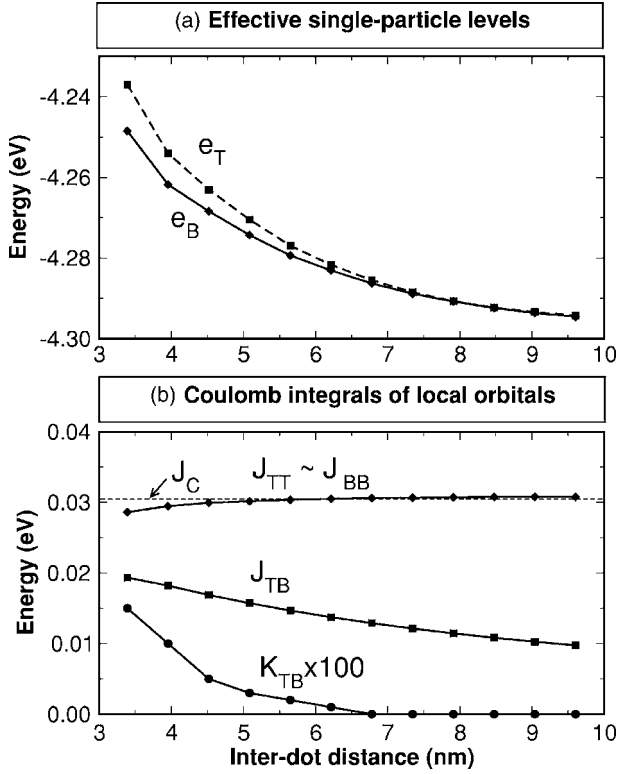
FIG. 7. (a) Effective single-particle energy levels of s orbitals localized on the top (e_T) and bottom (e_B) dots. (b) Intradot Coulomb energy J_{TT}, J_{BB}, interdot Coulomb energy J_{TB} and interdot exchange energy K_{TB} (magnified by a factor 100). The dashed line gives the single-dot s orbital self-Coulomb energy J_C.

$$e_\eta = \langle \chi_\eta | \hat{T} | \chi_\eta \rangle = \sum_i \mathcal{U}^*_{\eta,i} \mathcal{U}_{\eta,i} \epsilon_i, \quad (15)$$

$$t_{\eta_1 \eta_2} = \langle \chi_{\eta_1} | \hat{T} | \chi_{\eta_2} \rangle = \sum_i \mathcal{U}^*_{\eta_1,i} U_{\eta_2,i} \epsilon_i, \quad (16)$$

where ϵ_i is the single-particle level of the ith *molecular* orbital, and $\hat{T}$ is kinetic energy operator. Using the transformation of Eq. (15), Eq. (16), and Eq. (B2), we calculate all parameters of Eq. (13). Figure 7(a) shows the effective single-dot energy of the "s" orbitals obtained in the Wannier representation for both top and bottom dots. We see that the effective single-dot energy levels increase rapidly for small d. Furthermore, the energy levels for the top and bottom orbitals are split due to the strain asymmetry between the two dots. We compute the Coulomb energies J_{TT}, J_{BB} of the "s" orbitals on both top and bottom dots, and the interdot Coulomb and exchange energies J_{TB} and K_{TB} and plot these quantities in Fig. 7(b). Since J_{TT} and J_{BB} are very similar, we plot only J_{TT}. As we can see, the Coulomb energies of the dot-centered orbitals are very close to the Coulomb energy of the s orbitals of an *isolated* single dot (dashed line). The interdot Coulomb energy J_{TB} has comparable amplitude to J_{TT} and decays slowly with distance, and remain very significant, even at large separations. However, the exchange energy between the orbitals localized on the top and bottom dot K_{TB} is extremely small even when the dots are very close.

2. "First-principles" Hubbard model and Heisenberg model: Level 4

In level-4 approximation, we use only the "s" orbital in each dot. Figure 1(b) shows all possible many-body basis functions of two electrons, where the top and bottom dots are denoted by "T" and "B," respectively. The Hamiltonian in this basis set is

Coulomb integrals in the new basis set are given by Eq. (B2), while other quantities including the effective single-particle levels e_η for the ηth dot-centered orbital, and the coupling between the η_1th and η_2th orbitals $t_{\eta_1 \eta_2}$ can be obtained from

$$H = \begin{pmatrix}
e_T + e_B + J_{TB} - K_{TB} & 0 & 0 & 0 & 0 & 0 \\
0 & e_T + e_B + J_{TB} - K_{TB} & 0 & 0 & 0 & 0 \\
0 & 0 & e_T + e_B + J_{TB} & -K_{TB} & t - \widetilde{\Gamma}^{TB}_{BB} & t - \widetilde{\Gamma}^{TB}_{TT} \\
0 & 0 & -K_{TB} & e_T + e_B + J_{TB} & -t + \widetilde{\Gamma}^{TB}_{BB} & -t + \widetilde{\Gamma}^{TB}_{TT} \\
0 & 0 & t - \widetilde{\Gamma}^{BB}_{TB} & -t + \widetilde{\Gamma}^{BB}_{TB} & 2e_B + J_{BB} & 0 \\
0 & 0 & t - \widetilde{\Gamma}^{TT}_{TB} & -t + \widetilde{\Gamma}^{TT}_{TB} & 0 & 2e_T + J_{TT}
\end{pmatrix}, \quad (17)$$

where $t = t_{TB}$ and to simplify the notation, we ignore the orbital index "s." If we keep all the matrix elements, the description using the molecular basis of Fig. 1(a) and the dot localized basis of Fig. 1(b) are equivalent, since they are connected by unitary transformations. We now simplify Eq. (17) by ignoring the off-diagonal Coulomb integrals. The

resulting Hamiltonian is the single-band Hubbard model. Unlike level-3 theory, in this case, ignoring off-diagonal Coulomb integrals (but keeping hopping) can still give qualitatively correct results, due to the fact that off-diagonal Coulomb integrals such as $\widetilde{\Gamma}^{BB}_{TB} \ll t$, and the correlation is mainly carried by interdot hopping t. We can further simplify the

model by assuming $e_T = e_B = \epsilon$; $J_{TT} = J_{BB} = U$; and let $J_{TB} = V$, $K_{TB} = K$. We can then solve the simplified eigenvalue equation analytically. The eigenvalues of the above Hamiltonian are (in order of increasing energy):

(i) ground-state singlet $^1\Sigma_g^{(a)}$,

$$E = 2\epsilon + \frac{1}{2}[U + V + K - \sqrt{16t^2 + (U - V - K)^2}]; \quad (18)$$

(ii) triplet states (threefold degenerate) $^3\Sigma_u$,

$$E = 2\epsilon + V - K; \quad (19)$$

(iii) singlet $^1\Sigma_u$,

$$E = 2\epsilon + U; \quad (20)$$

(iv) singlet $^1\Sigma_g^{(b)}$,

$$E = 2\epsilon + \frac{1}{2}[U + V + K + \sqrt{16t^2 + (U - V - K)^2}]. \quad (21)$$

In the Hubbard limit where Coulomb energy $U \gg t$, the singlet-triplet splitting $J_{S-T} = E(^3\Sigma) - E(^1\Sigma_g) \sim 4t^2/(U-V)$, which reduces the model to the Heisenberg model

$$H = \frac{4t^2}{U - V}\vec{S}_T \cdot \vec{S}_B, \quad (22)$$

where $\vec{S}_T$ and $\vec{S}_B$ are the spin vectors on the top and bottom dots. The Heisenberg model gives the correct order for singlet and triplet states. The singlet-triplet splitting $J_{S-T} = 4t^2/(U-V)$ is plotted in Fig. 5(c) and compared to the results from all-bound-state CI calculations (level 1), and single-configuration approximations (level 3). As we can see, at $d > 6.5$ nm, the agreement between the Heisenberg model with CI is good, but the Heisenberg model greatly overestimates J_{S-T} at $d < 6$ nm.

E. Comparison of pair-correlation functions for level-1 to 4 theories

In the previous sections, we compared the energy levels of two-electron states in several levels of approximations to all-bound-state CI results (level 1). We now provide further comparison of level-1–4 theories by analyzing the pair-correlation functions and calculating the electron-electron entanglement at different levels of approximations.

In Fig. 8 we show the pair-correlation functions of Eq. (6) for the $^1\Sigma_g^{(a)}$ and $^1\Sigma_g^{(b)}$ states at $d \sim 7$ nm for level-1 and level-3 theories. The correlation functions give the probability of finding the second electron when the first electron is fixed at the position shown by the arrows at the center of the bottom dot (left-hand side of Fig. 8) or the top dot (right-hand side of Fig. 8). Level-1 and level-2 theories give correlation-induced electron localization at large d: for the $^1\Sigma_g^{(a)}$ state, the two electrons are localized on different dots, while for the $^1\Sigma_g^{(b)}$ state, both electrons are localized on the same dot.[24] In contrast, level-3 theory shows delocalized states because of the lack of configuration mixing. This problem is shared by RHF and LSD approximations.
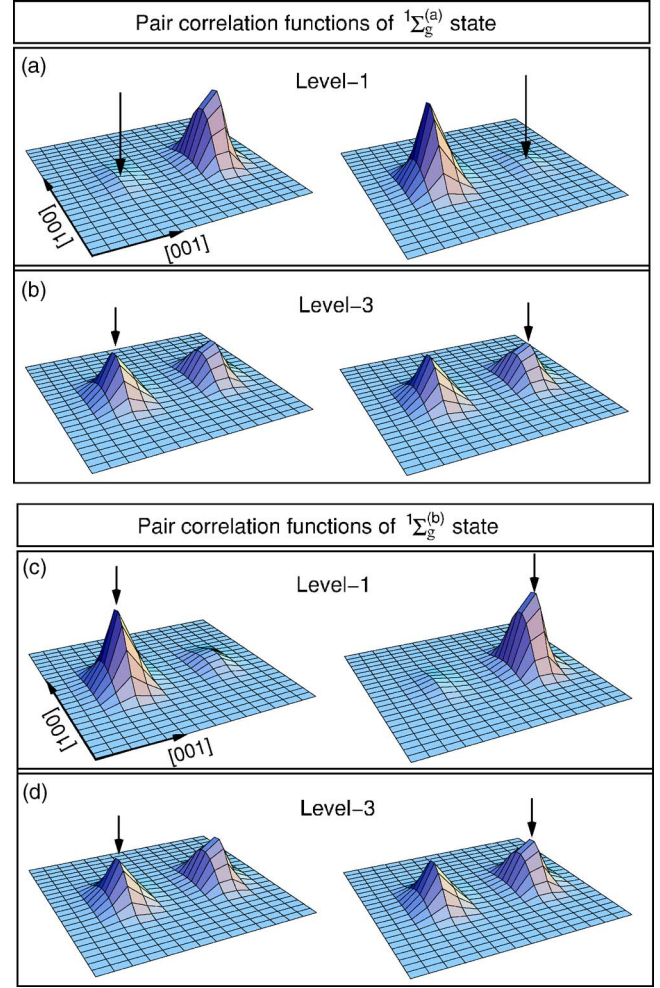

FIG. 8. (Color online) Comparison of pair-correlation functions calculated from (a) level-1 and (b) level-3 theory for the $^1\Sigma_g^{(a)}$ state and (c) level-1 and (d) level-3 theory for the $^1\Sigma_g^{(b)}$ state at $d \sim 7$ nm. On the left-hand side, the first electron is fixed at the center of the bottom dot, while on the right-hand side, the first electon is fixed at the center of the top dot, as indicated by the arrows.

F. Comparison of the degree of entanglement for levels-1 to 4 theories

The DOE of the four "Σ" states are plotted in Fig. 9 for level-1, level-3, and level-4 theories; the DOEs of level-2 theory are virtually identical to those of level-1 theory, and are therefore not plotted. We see that the Hubbard model has generally reasonable agreement with level-1 theory while the DOEs calculated from level-3 and level-4 (Heisenberg model) theories deviate significantly from the level-1 theory, which is addressed below.

(i) *The $^1\Sigma_g^{(a)}$ state*: The level-1 theory [Fig. 9(a)], shows that the DOE of $^1\Sigma_g^{(a)}$ increases with d and approaches 1 at large d. The Hubbard model of level-4 theory [Fig. 9(c)] gives qualitatively correct DOE for this state except for some details. However, level-3 theory [Fig. 9(b)] gives DOE $S = 0$ because the wave function of $^1\Sigma_g^{(a)}$ is a single Slater determinant $|e\rangle$ [see Eq. (9)]. For the same reason, the DOEs
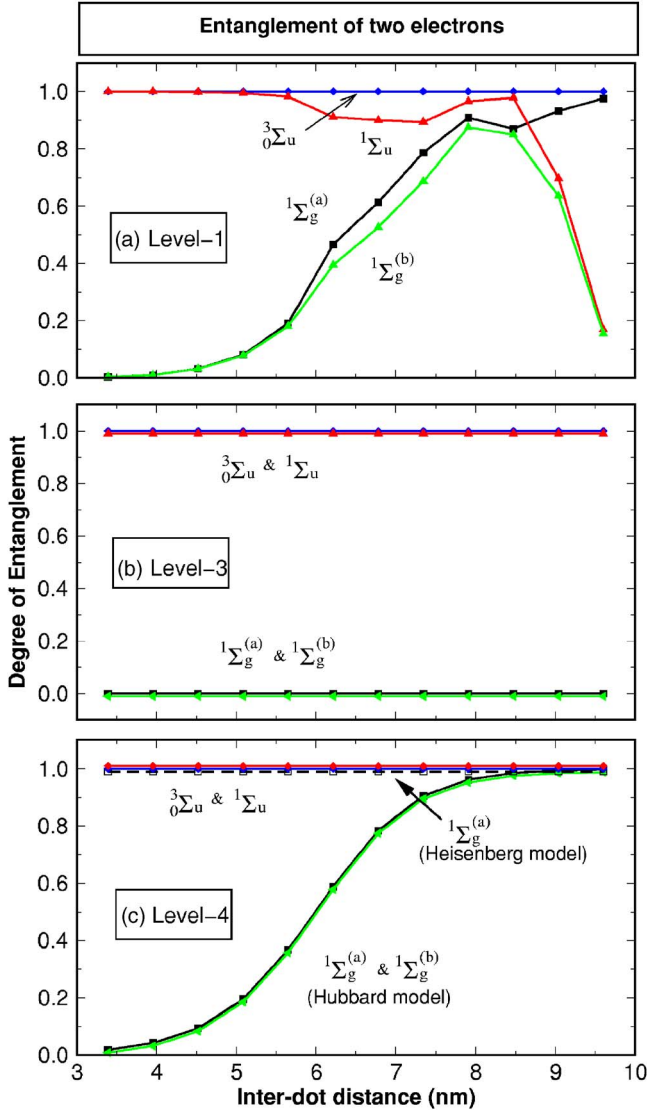
FIG. 9. (Color online) Comparison of the DOE calculated from (a) level-1, (b) level-3, and (c) level-4 theories for two-electron states. In panel (c), both the DOE of the Hubbard model (solid lines) and of the Heisenberg model for $^1\Sigma_g^{(a)}$ state (dashed line) are shown.

of the $^1\Sigma_g^{(a)}$ state in RHF and LSD approximations are also zero as a consequence of lack of correlation. In contrast, the Heisenberg model of level-4 theory gives $\mathcal{S}(^1\Sigma_g^{(a)})=1$. This is because the Heisenberg model assumes that the both electrons are localized on different dots with zero double occupancy, and thus overestimates the DOE.[24,45]

(ii) *The* $^1\Sigma_g^{(b)}$ *state*: The Hubbard model gives the DOE of the $^1\Sigma_g^{(b)}$ state identical to that of $^1\Sigma_g^{(a)}$ state. This is different from the result of level-1 theory, especially at large inter-dot separations. The difference comes from the assumption in the Hubbard model that the energy levels and wave functions on the top dot and on the bottom dot are identical while as discussed in Ref. 24, the wave functions are actually asymmetric due to inhomogeneous strain in the real system. At $d>8$ nm, the $^1\Sigma_g^{(b)}$ state is the supposition of $|E\rangle$ and $|F\rangle$ configurations in the Hubbard model leading to $\mathcal{S}=1$, while

in level-1 theory, the two electrons are both localized on the *top* dots ($|F\rangle$) at $d>9$ nm,[24] resulting in near zero entanglement. For the same reason discussed in (i), the level-3 theory gives $\mathcal{S}(^1\Sigma_g^{(b)})=0$.

(iii) *The* $^1\Sigma_u$ *state*: Both the level-3 theory and Hubbard model give $\mathcal{S}(^1\Sigma_u)=1$. However, the $\mathcal{S}(^1\Sigma_u)$ of the level-1 theory has more features as the consequence of the asymmetry of the system. In contrast to the $^1\Sigma_g^{(b)}$ state, in the $^1\Sigma_u$ state, both electrons are localized on the *bottom* dot leading to near zero entanglement at $d>9$ nm.

(iv) *The* $^3\Sigma_u$ *state*: All levels of theories give very close results of DOE for the $^3_0\Sigma_u$ state. Actually, in level-1 theory, the DOE of the $^3_0\Sigma_u$ state is only slightly larger than 1, indicating weak entanglement of the σ and π orbitals (the maximum entanglement one can get from the total of six orbitals is $\mathcal{S}_{max}=\log_2 6$), while in all other theories (including the level-2 theory) they are exactly 1 since these theories include only two σ orbitals. The small coupling between σ and π orbitals is desirable for quantum computation, which requires the qubits states to be decoupled from other states.

IV. SUMMARY

We have shown the energy spectrum, pair-correlation functions, and degree of entanglement of two-electron states in self-assembled InAs/GaAs quantum dot molecules via all-bound-state configuration interaction calculations and compared these quantities in different levels of approximations. We find that the correlation between electrons in the top and bottom dot is crucial to get the qualitative correct results for both the singlet-triplet splitting and the degree of entanglement. The single-configuration approximation and similar theories such as RHF and LSD all suffer from lack of correlation and thus give incorrect ground state, singlet-triplet splitting J_{S-T}, and degree of entanglement. Highly simplified models, such as the Hubbard model, gives qualitatively correct results for the ground state and J_{S-T}, while the Heisenberg model only gives similar results at large d. These two models are written in the dot-centered basis, where the correlation between the top and bottom dots are carried by the single-particle tunneling. However, as a consequence of ignoring the asymmetry present in the real system, the degree of entanglement calculated from the Hubbard model deviates significantly from realistic atomic calculations. Moreover, the Heisenberg model greatly overestimates the degree of entanglement of the ground state as a consequence of further ignoring the electron double occupancy in the dot molecule.

ACKNOWLEDGMENTS

APPENDIX A: DEGREE OF ENTANGLEMENT FOR TWO ELECTRONS

The entanglement is characterized by the fact that the many-particle wave functions cannot be factorized as a direct

product of single-particle wave functions. An entangled system displays nonlocality which is one of the properties that distinguishes it from classic systems. So far, the only well established theory of entanglement pertains to two *distinguishable* particles,[32,34] (e.g., electron and hole). For a system made of two distinguishable particles (A, B), the entanglement can be quantified by von Neumann entropy of the partial density matrix of either A or B,[31–33]

$$\mathcal{S}(A,B) = -\text{Tr}(\rho_A \log_2 \rho_A) = -\text{Tr}(\rho_B \log_2 \rho_B), \quad \text{(A1)}$$

where $\mathcal{S}(A,B)$ is the DOE of the state. ρ_A and ρ_B are the reduced density matrices for subsystems A and B. An alternative way to define the DOE for two distinguishable particles is through a Schmidt decomposition, where two-nonidentical-particle wave functions are written in an biorthogonal basis,

$$\Psi(A,B) = \sum_i \lambda_i |i_A\rangle \otimes |i_B\rangle, \quad \text{(A2)}$$

with $\lambda_i \geq 0$ and $\Sigma_i \lambda_i^2 = 1$. The number of nonzero λ_i is called the Schmidt rank. For a pure state $\Psi(A,B)$ of the composite system (A, B), we have

$$\rho_A = \sum_i \lambda_i^2 |i_A\rangle\langle i_A|, \quad \text{(A3)}$$

$$\rho_B = \sum_i \lambda_i^2 |i_B\rangle\langle i_B|.$$

It is easy to show from Eq. (A1) that the DOE for the two distinguishable particles is

$$\mathcal{S}(A,B) = -\sum_i \lambda_i^2 \log_2 \lambda_i^2. \quad \text{(A4)}$$

We see from Eq. (A2) that when and only when the Schmidt rank equals 1, the two-particle wave function can be written as a direct product of two single-particle wave functions. In this case, we have $\lambda = 1$, and $\mathcal{S}(A,B) = 0$ from Eq. (A4).

A direct generalization of DOE of Eq. (A4) for two identical particles is problematic. Indeed, there is no general way to define the subsystem A and B for two *identical* particles. More seriously, since two-particle wave functions for identical particles are nonfactorable due to their built-in symmetry, one may tend to believe that all two identical fermions (or Bosons) are in an entangled Bell state.[32] However, inconsistency comes up in the limiting cases. For example, suppose that two electrons are localized on each of the two sites A and B that are far apart, where the two electrons can be treated as *distinguishable* particles by assigning A and B to each electron, respectively. A pure state Ψ that has the spin up for A electron and spin down for B electron is $\Psi(\mathbf{x}_1, \mathbf{x}_2) = 1/\sqrt{2}[\phi_{A\uparrow}(\mathbf{x}_1)\phi_{B\downarrow}(\mathbf{x}_2) - \phi_{A\uparrow}(\mathbf{x}_2)\phi_{B\downarrow}(\mathbf{x}_1)]$. At first sight, because of the antisymmetrization, it would seem that the two electron states cannot be written as a direct product of two single-particle wave functions, so this state is maximally entangled. However, when the overlap between two wave functions is negligible, we can treat these two particles as if they were distinguishable particles and ignore the antisymmetrization without any physical effect, i.e.,

$\Psi(\mathbf{x}_1, \mathbf{x}_2) = \phi_{A\uparrow}(\mathbf{x}_1)\phi_{B\downarrow}(\mathbf{x}_2)$. In this case, apparently the two electrons are *unentangled*. More intriguingly, in quantum theory, *all* fermions have to be antisymmetrized even for *nonidentical* particles, which does not mean they are entangled.

To solve this obvious inconsistency, alternative measures of the DOE of two fermions have been proposed and discussed recently,[35–41] but no general solution has been widely accepted as yet. Schliemann *et al.*[35] proposed using Slater decomposition to characterize the entanglement (or, the so-called "quantum correlation" in Ref. 35) of two fermions as a counterpart of the Schmidt decomposition for distinguishable particles. Generally a two-particle wave function can be written as

$$\Psi = \sum_{i,j} \omega_{ij} |i\rangle \otimes |j\rangle, \quad \text{(A5)}$$

where $|i\rangle$, $|j\rangle$ are the single-particle orbitals. The coefficient ω_{ij} must be antisymmetric for two fermions. It has been shown in Refs. 35 and 42 that one can do a Slater decomposition of ω_{ij} similar to the Schmidt decomposition for two nonidentical particles. It has been shown that ω can be block diagonalized through a unitary rotation of the single-particle states,[35,42] i.e.,

$$\omega' = U\omega U^\dagger = \text{diag}[Z_1, Z_2, \ldots, Z_r, Z_0], \quad \text{(A6)}$$

where

$$Z_i = \begin{pmatrix} 0 & z_i \\ -z_i & 0 \end{pmatrix}. \quad \text{(A7)}$$

and $Z_0 = 0$. Furthermore, $\Sigma_i z_i^2 = 1$, and z_i is a non-negative real number. A more concise way to write down the state Ψ is to use the second quantization representation,

$$\Psi = \sum_i z_i f_{2i-1}^\dagger f_{2i}^\dagger |0\rangle, \quad \text{(A8)}$$

where $f_{2i-1}^\dagger$ and $f_{2i}^\dagger$ are the creation operators for modes $2i-1$ and $2i$. Following Ref. 42, it is easy to prove that z_i^2 are eigenvalues of $\omega^\dagger \omega$. The number of nonzero z_i is called the Slater rank.[35] It has been argued in Ref. 35 that if the wave function can be written as single Slater determinant, i.e., the Slater rank equals 1, the so-called quantum correlation of the state is zero. The quantum correlation function defined in Ref. 35 has similar properties, but nevertheless is inequivalent to the usual definition of DOE.

Here, we propose a generalization of the DOE of Eq. (A4) to two fermions, using the Slater decompositions,

$$\mathcal{S} = -\sum_i z_i^2 \log_2 z_i^2. \quad \text{(A9)}$$

The DOE measure of Eq. (A9) has the following properties:

(i) This DOE measure is similar to the one proposed by Paškauskas *et al.*[36] and Li *et al.*,[39] except that a different normalization condition is used. In our approach, the state of Slater rank 1 is unentangled, i.e., $\mathcal{S} = 0$. In contrast, Paškauskas *et al.*[36] and Li *et al.*[39] concluded that the unentangled state has $\mathcal{S} = \ln 2$, which is contradictory to the fact that for distinguishable particles, an unentangled state must have $\mathcal{S}$

=0. In our approach, the maximum entanglement that a state can have is $\mathcal{S}=\log_2 N$, where N is the number of single-particle states.

(ii) The DOE measure of Eq. (A9) is invariant under any unitary transformation of the single-particle orbitals. Suppose there is coefficient matrix ω, a unitary transformation of the single-particle basis leads to a new matrix $\omega'=U\omega U^\dagger$ and $\omega'^\dagger\omega'=U\omega^\dagger\omega U^\dagger$. Obviously, this transformation would not change the eigenvalues of $\omega^\dagger\omega$, i.e., would not change the entanglement of the system.

(iii) The DOE of Eq. (A9) for two fermions reduces to the usual DOE measure of Eq. (A4) for two *distinguishable* particles in the cases of zero double occupation of same site (while the DOE measure proposed by Paškauskas et al.[36] and Li et al.[39] does not). This can be shown as follows: since the DOE of measure Eq. (A9) is basis independent, we can choose a dot-localized basis set [which in the case here is the top (T) and bottom (B) dots, Fig. 1(b)], such that the anti-symmetric ω matrix in the dot-localized basis has four blocks,

$$\omega = \begin{pmatrix} \omega_{TT} & -\omega_{TB}^\dagger \\ \omega_{TB} & \omega_{BB} \end{pmatrix}, \qquad (A10)$$

where ω_{TT} is the coefficient matrix of two electrons both occupying the top dot, etc. If the double occupation is zero, i.e., two electrons are always on different dots, we have matrices $\omega_{TT}=\omega_{BB}=0$. It is easy to show that $\omega^\dagger\omega$ has two identical sets of eigenvalues z_i^2, each are the eigenvalues of $\omega_{BT}^\dagger\omega_{BT}$. On the other hand, if we treat the two electrons as distinguishable particles, and ignore the antisymmetrization in the two-particle wave functions, we have $\rho_B=\omega_{TB}^\dagger\omega_{TB}$ and $\rho_T=\omega_{BT}^\dagger\omega_{BT}$. It is straightforward to show that in this case Eqs. (A9) and (A4) are equivalent.

APPENDIX B: CONSTRUCTION OF DOT-CENTERED ORBITALS

When we solve the single-particle Eq. (1) for the QDM, we get a set of molecular orbitals. However, sometimes we need to discuss the physics in a dot-localized basis set. The dot-localized orbitals χ_η can be obtained from a unitary rotation of molecular orbitals,

$$\chi_\eta = \sum_{i=1}^N \mathcal{U}_{\eta,i}\psi_i, \qquad (B1)$$

where ψ_i is the ith molecular orbital, and $\mathcal{U}$ is a unitary matrix, i.e., $\mathcal{U}^\dagger\mathcal{U}=I$. To obtain a set of well localized orbitals, we require that the unitary matrix $\mathcal{U}$ maximizes the total orbital self-Coulomb energy. The orbitals fulfilling the requirement are approximately invariant under the changes due to coupling between the dots.[44] For a given unitary matrix $\mathcal{U}$, the Coulomb integrals in the rotated basis are

$$\tilde{\Gamma}_{\eta_3,\eta_4}^{\eta_1,\eta_2} = \sum_{i,j,k,l} \mathcal{U}_{\eta_1,i}^* \mathcal{U}_{\eta_2,j}^* \mathcal{U}_{\eta_3,k} \mathcal{U}_{\eta_4,l} \Gamma_{k,l}^{i,j}, \qquad (B2)$$

where $\Gamma_{k,l}^{i,j}$ are the Coulomb integrals in the molecular basis. Thus the total self-Coulomb energy for the orbitals $\{\chi_\eta\}$ is

$$U_{\text{tot}} = \sum_\eta \tilde{\Gamma}_{\eta,\eta}^{\eta,\eta} = \sum_\eta \sum_{i,j,k,l} \mathcal{U}_{\eta,i}^* \mathcal{U}_{\eta j}^* \mathcal{U}_{\eta,k} \mathcal{U}_{\eta,l} \Gamma_{k,l}^{i,j}. \qquad (B3)$$

The procedure of finding the unitary matrix $\mathcal{U}$ that maximizes U_{tot} is similar to the procedure given in Ref. 46 where the maximally localized Wannier functions for extended systems are constructed using a different criteria. Starting from $\mathcal{U}=I$, we find a new $\mathcal{U}=I+\delta\epsilon$ that increases U_{tot}. To keep the new matrix unitary, we require $\delta\epsilon$ to be a small anti-Hermitian matrix. It is easy to prove that

$$G_{i,j} \equiv \frac{\delta U_{\text{tot}}}{\delta\epsilon_{j,i}} = \Gamma_{i,j}^{j,j} + \Gamma_{j,i}^{j,j} - \Gamma_{i,i}^{i,j} - \Gamma_{i,i}^{j,i} \qquad (B4)$$

and to verify that $G_{i,j}=-G_{j,i}^*$. By choosing $\delta\epsilon_{i,j}=-\epsilon G_{i,j}$, where ϵ is a small real number, we always have (to the first-order of approximation) $\Delta U_{\text{tot}}=\epsilon\|G\|\geq 0$, i.e., the procedure always increases the total self-Coulomb energy. To keep the strict unitary character of the $\mathcal{U}$ matrices in the procedure, the $\mathcal{U}$ matrices are actually updated as $\mathcal{U}\leftarrow\mathcal{U}\exp(-\epsilon G)$, until the localization is achieved.

[1] M. Pi, A. Emperador, M. Barranco, F. Garcias, K. Muraki, S. Tarucha, and D. G. Austing, Phys. Rev. Lett. **87**, 066801 (2001).

[2] M. Rontani, S. Amaha, K. Muraki, F. Manghi, E. Molinari, S. Tarucha, and D. G. Austing, Phys. Rev. B **69**, 085327 (2004).

[3] F. R. Waugh, M. J. Berry, D. J. Mar, R. M. Westervelt, K. L. Campman, and A. C. Gossard, Phys. Rev. Lett. **75**, 705 (1995).

[4] M. Bayer, P. Hawrylak, K. Hinzer, S. Fafard, M. Korkusinski, Z. R. Wasilewski, O. Stern, and A. Forchel1, Science **291**, 451 (2001).

[5] D. Loss and D. P. DiVincenzo, Phys. Rev. A **57**, 120 (1998).

[6] R. C. Ashoori, H. L. Stormer, J. S. Weiner, L. N. Pfeiffer, S. J. Pearton, K. W. Baldwin, and K. W. West, Phys. Rev. Lett. **68**, 3088 (1992).

[7] A. T. Johnson, L. P. Kouwenhoven, W. de Jong, N. C. van der Vaart, C. J. P. M. Harmans, and C. T. Foxon, Phys. Rev. Lett.

69, 1592 (1992).

[8] S. Tarucha, D. G. Austing, T. Honda, R. J. van der Hage, and L. P. Kouwenhoven, Phys. Rev. Lett. **77**, 3613 (1996).

[9] G. Burkard, D. Loss, and D. P. DiVincenzo, Phys. Rev. B **59**, 2070 (1999).

[10] H. Tamura, Physica B **249-251**, 210 (1998).

[11] C. Yannouleas and U. Landman, Phys. Rev. Lett. **82**, 5325 (1999).

[12] X. Hu and S. DasSarma, Phys. Rev. A **61**, 062301 (2000).

[13] S. Nagaraja, J. P. Leburton, and R. M. Martin, Phys. Rev. B **60**, 8759 (1999).

[14] B. Partoens and F. M. Peeters, Phys. Rev. Lett. **84**, 4433 (2000).

[15] M. Rontani, F. Troiani, U. Hohenester, and E. Molinari, Solid State Commun. **119**, 309 (2001).

[16] C. Yannouleas and U. Landman, Eur. Phys. J. D **16**, 373 (2001).

[17] C. Yannouleas and U. Landman, Int. J. Quantum Chem. **90**, 699 (2002).

[18] W. A. Goddard, T. H. Dunning, W. J. Hunt, and P. J. Hay, Acc. Chem. Res. **6**, 368 (1973).

[19] D. Das (unpublished).

[20] T. Ota, M. Stopa, M. Rontani, T. Hatano, K. Yamada, S. Tarucha, H. Song, Y. Nakata, T. Miyazawa, T. Ohshima, and N. Yokoyama, Superlattices Microstruct. **34**, 159 (2003).

[21] T. Ota, K. Ono, M. Stopa, T. Hatano, S. Tarucha, H. Z. Song, Y. Nakata, T. Miyazawa, T. Ohshima, and N. Yokoyama, Phys. Rev. Lett. **93**, 066801 (2004).

[22] L. W. Wang, A. J. Williamson, A. Zunger, H. Jiang, and J. Singh, Appl. Phys. Lett. **76**, 339 (2000).

[23] G. Bester, J. Shumway, and A. Zunger, Phys. Rev. Lett. **93**, 047401 (2004).

[24] L. He, G. Bester and A. Zunger, Phys. Rev. B **72**, 081311(R) (2005).

[25] P. N. Keating, Phys. Rev. **145**, 637 (1966).

[26] J. L. Martins and A. Zunger, Phys. Rev. B **30**, 6217 (1984).

[27] A. J. Williamson, L.-W. Wang, and A. Zunger, Phys. Rev. B **62**, 12963 (2000).

[28] L. He, G. Bester, and A. Zunger, Phys. Rev. B **70**, 235316 (2004).

[29] L.-W. Wang and A. Zunger, Phys. Rev. B **59**, 15806 (1999).

[30] A. Franceschetti, H. Fu, L.-W. Wang, and A. Zunger, Phys. Rev. B **60**, 1819 (1999).

[31] C. H. Bennett, H. J. Bernstein, S. Popescu, and B. Schumacher, Phys. Rev. A **53**, 2046 (1996).

[32] M. A. Nielsen and I. L. Chuang, *Quantum Computation and Quantum Information* (Cambridge University Press, Cambridge, England, 2000).

[33] A. Wehrl, Rev. Mod. Phys. **50**, 221 (1978).

[34] C. H. Bennett, D. P. DiVincenzo, J. A. Smolin, and W. K. Wootters, Phys. Rev. A **54**, 3824 (1996).

[35] J. Schliemann, J. I. Cirac, M. Kuś, M. Lewenstein, and D. Loss, Phys. Rev. A **64**, 022303 (2001).

[36] R. Paškauskas and L. You, Phys. Rev. A **64**, 042310 (2001).

[37] G. C. Ghirardi and L. Marinatto, Phys. Rev. A **70**, 012109 (2004).

[38] H. M. Wiseman and J. A. Vaccaro, Phys. Rev. Lett. **91**, 097902 (2003).

[39] Y. S. Li, B. Zeng, X. S. Liu, and G. L. Long, Phys. Rev. A **64**, 054302 (2001).

[40] P. Zanardi, Phys. Rev. A **65**, 042101 (2002).

[41] Y. Shi, Phys. Rev. A **67**, 024301 (2003).

[42] C. N. Yang, Rev. Mod. Phys. **34**, 694 (1962).

[43] J. J. Palacios and P. Hawrylak, Phys. Rev. B **51**, 1769 (1995).

[44] C. Edmiston and K. Ruedenberg, Rev. Mod. Phys. **35**, 457 (1963).

[45] J. Schliemann, D. Loss, and A. H. MacDonald, Phys. Rev. B **63**, 085311 (2001).

[46] N. Marzari and D. Vanderbilt, Phys. Rev. B **56**, 12847 (1997).